CHEMISTRY
A EUROPEAN JOURNAL

DOI: 10.1002/chem.200601885

Dynamics and Counterion-Dependence of the Structures of Weakly Bound Ag^+–P_4S_3 Complexes

Ines Raabe,[a] Sasa Antonijevic,*[b] and Ingo Krossing*[a]

Abstract: In an earlier publication (*J. Am. Chem. Soc.* **2002**, *124*, 7111) we showed that polymeric cationic $[Ag(P_4S_3)_n]^+$ complexes ($n=1$, 2) are accessible if partnered with a suitable weakly coordinating counterion of the type $[Al(OR^F)_4]^-$ (OR^F: poly- or perfluorinated alkoxide). The present work addresses the following questions that could not be answered in the initial report: How many P_4S_3 cages can be bound to a Ag^+ ion? Why are these complexes completely dynamic in solution in the ^{31}P NMR experiments? Can these dynamics be frozen out in a low-temperature ^{31}P MAS NMR experiment? What are the principal binding sites of the P_4S_3 cage towards the Ag^+ ion? What are likely other isomers on the $[Ag(P_4S_3)_n]^+$ potential energy surface? Counterion influence: Reactions of P_4S_3 with $Ag[Al\{OC(CH_3)(CF_3)_2\}_4]$ (Ag[hftb]) and $Ag[\{(CF_3)_3CO\}_3Al\text{-}F\text{-}Al\{OC(CF_3)_3\}_3]$ (Ag[al-f-al]) gave $[(P_4S_3)Ag[hftb]]_\infty$ (**7**) as a molecular species, whereas $[Ag_2(P_4S_3)_6]^{2+}[al\text{-}f\text{-}al]^-_2$ (**8**) is an isolated 2:1 salt. We suggest that a maximum of three P_4S_3 cages may be bound on average to an Ag^+ ion. Only isolated dimeric dications are formed with the largest cation, but polymeric species are obtained with all other smaller aluminates. Thermodynamic Born–Haber cycles, DFT calculations, as well as solution NMR and ESI mass spectrometry indicate that **8** exhibits an equilibrium between the dication $[Ag_2(P_4S_3)_6]^{2+}$ (in the solid state) and two $[Ag(P_4S_3)_3]^+$ monocations (in the gas phase and in solution). Dynamics: ^{31}P MAS NMR spectroscopy showed these solid adducts to be highly dynamic, to an extent that the $^2J_{P,P}$ coupling within the cages could be resolved (*J*-res experiment). This is supported by DFT calculations, which show that the extended PES of $[Ag(P_4S_3)_n]^+$ ($n=1$–3) and $[Ag_2(P_4S_3)_2]^+$ is very flat. The structures of α- and γ-P_4S_3 were redetermined. Their variable-temperature ^{31}P MAS NMR spectra are discussed jointly with those of all four currently known $[Ag(P_4S_3)_n]^+$ adducts with $n=1$, 2, and 3.

Keywords: NMR spectroscopy · phosphorus · silver · sulfur · weakly coordinating anions

Introduction

Lewis acid–base adducts of small inorganic cluster molecules such as P_4, P_5^-, $P_3N_3Cl_6$, S_8, or P_4S_3 are of fundamental interest for coordination chemistry, although not many examples of such complexes are currently known.[1–6] The first P_4S_3 complex, $[Mo(CO)_5(P_4S_3)]$, was reported by Cordes and co-workers in 1974.[7] In this compound, as well as in the rare later examples, such as $[(np_3)Ni(P_4S_3)]$ [1,2] (np_3: tris(2-(diphenylphosphino)ethyl)amine) or $(P_4S_3)(BX_3)$ (X: Br, I),[8] the P_4S_3 cage is bound through the apical P atom. When P_4S_3 acted as a bridging ligand, oxidative addition and bond cleavage of P–P and P–S bonds were observed.[9] Generally, the P_4S_3 molecule is likely to be prone to degradation when allowed to react with transition-metal compounds. This fragmentation is supposed to proceed both through the S and/or P atoms, as indicated by the respective reaction products.[10,11]

[a] Dipl.-Chem. I. Raabe, Prof. Dr. I. Krossing
Albert-Ludwigs-Universität Freiburg
Institut für Anorganische und Analytische Chemie
Albertstrasse 21, 79104 Freiburg i. Br. (Germany)
Fax: (+49) 761-203-6001
E-mail: krossing@uni-freiburg.de

[b] Dr. S. Antonijevic
Ecole Polytechnique Fédérale de Lausanne
Institut des Sciences et Ingénierie Chimiques
Batochimie, 1015 Lausanne (Switzerland)
Fax : (+41) 21-693-9355
E-mail: sasa.antonijevic@epfl.ch

Supporting information (additional structural information about these compounds and properties of all calculated species (*x*,*y*,*z* coordinates, ZPE, vibrational frequencies, NMR shielding tensors, solvation energies)) for this article is available on the WWW under http://www.chemeurj.org/ or from the authors.

We were interested in studying models for the primary steps of such degradation reactions in more detail. Ag^+ is a soft d^{10} transition metal and, as such, will seek the same reactive sites in P_4S_3 than other more reactive transition-metal fragments that usually induce degradation. Yet, these Ag^+–P_4S_3 complexes are only weakly bound and not accessible with normal counterions. One method to obtain such weak transition-metal complexes uses solid-state reaction conditions and CuI as matrix, for example, $[(CuI)_3P_4S_4]$.[12] Another approach is the use of *w*eakly *c*oordinating *a*nions (WCAs), which are ideal counterions for stabilizing weakly bound cationic Lewis acid–base adducts,[13] such as, $[Ag(P_4)_2]^+$,[5,6] $[Ag(S_8)_2]^+$,[1] $[Au(Xe)_4]^+$,[14] $[Ag(P_3N_3Cl_6)_n]^+$,[3] $[Ag(C_2H_2)_n]^+$,[15] $\{[Ag\{Cp^*Fe(P_5)\}_2]^+\}_\infty$,[4] or $[Ag(C_2H_4)_n]^+$[16] as they minimize ionic interactions towards the cation due to charge delocalization. Thus, with the silver salts of the WCAs $[pftb]^-$ $(=[Al\{OC(CF_3)_3\}_4]^-)$[17] and $[hfip]^-$ $(=[Al\{OC(H)(CF_3)_2\}_4]^-)$[17] it was possible to obtain the Ag-(P_4S_3) adducts $[(P_4S_3)Ag[hfip]]$ (**1**) and $[Ag(P_4S_3)_2][pftb]$ (**2**).[18] Although both anions are rather similar, the structures of the adducts are very different. In fact, they are both polymeric, but whereas in $[(P_4S_3)Ag[hfip]]$ (**1**) molecular chains are formed, $[Ag(P_4S_3)_2][pftb]$ (**2**) has an ionic structure with homoleptic polymeric cations and isolated anions. In these species, unusual η^1-P_{basal} and η^1-S coordination was observed. At about the same time Peruzzini and co-workers also reported structures of P_4S_3 adducts with η^1-P_{basal} coordination.[19,20]

Here we report on the results of reactions with two new silver salts and the outcome of MAS NMR studies, extended DFT calculations, as well as a reassessment of the originally published compounds **1** and **2**.

Results and Discussion

The ^{31}P NMR spectra of **1** and **2** in solution (CD_2Cl_2) showed—even at −90 °C—only simple resonances that were nearly unchanged compared to those of free P_4S_3. This indicates weakly bound complexes with dynamic structures and low barriers for exchange. To obtain some insight into the likely and possible structures and energetics of such weak complexes, we initially describe possible minimum structures obtained by orienting DFT calculations, prior to proceeding with the experimental results.

Likely bonding sites of P_4S_3 in the $[Ag(P_4S_3)_n]^+$ (n=1, 2, 3) and $[Ag_2(P_4S_3)]^{2+}$ ions from DFT calculations: To investigate principal bonding sites of P_4S_3, quantum-chemical calculations at the (RI)-BP86/SV(P) level of theory were performed. For each $[Ag(P_4S_3)_n]^+$ ion (n=1–3), different coordination geometries and their relative Gibbs energies in the gas phase and in CH_2Cl_2 were calculated (standard conditions 298 K and 1.013 bar, COSMO model). The structures of the global minima are collected in Figure 1; the structures and relative energies of all considered isomers of these species are deposited. In the discussion, only isomers with relative energies of less than +25 kJ mol^{-1} are considered. This cut-off has been chosen because it is larger than the error bars of the quantum-chemical calculation, and still allows dynamic behavior in the solid state as well as in solution at −80 °C.

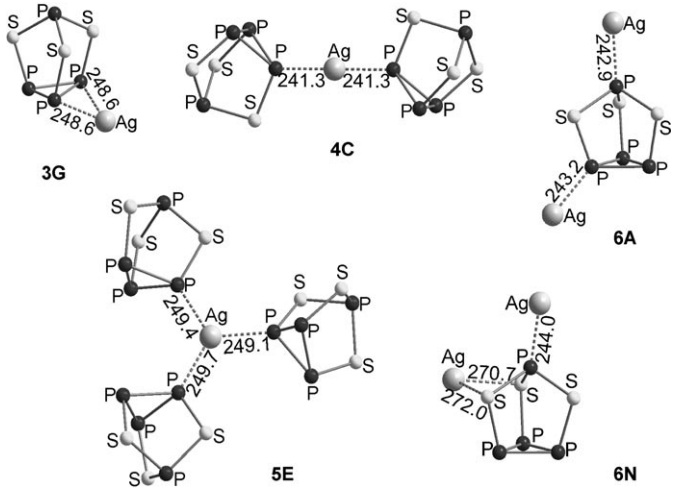

Figure 1. Geometries of the global minima (ΔG in the gas phase/ΔG in CH_2Cl_2) of $[Ag(P_4S_3)]^+$ (**3**), $[Ag(P_4S_3)_2]^+$ (**4**), $[Ag(P_4S_3)_3]^+$ (**5**), and $[Ag_2(P_4S_3)]^{2+}$ (**6**) at the (RI)-BP86-SV(P) level of theory. Complex **6A** is the global minimum in the gas phase and **6N** the minimum with inclusion of solvation (COSMO).

For compounds $[Ag(P_4S_3)]^+$ **3** the isomer **3G** with η^2-P_{basal}–P_{basal} coordination (Figure 1) is lowest in energy in the gas phase and in CH_2Cl_2; however, five other geometries are within 24.9 kJ mol^{-1} and are, with the exception of the η^3-coordinated **3H**, all local minima on the PES. Also for the model compounds $[Ag(P_4S_3)_2]^+$ **4**, the relative energies between the several other isomers differ only slightly (maximum 11.9 kJ mol^{-1}) from that of the minimum geometry **4C** (η^1-P_{basal}–P_{basal}, Figure 1). Interestingly, also for **4** ($[Ag(P_4S_3)_2]^+$) no η^3-coordinated species is a local minimum on the PES. This is also in agreement with the fact that no such P_4S_3 adduct has been observed so far. Moreover, it is clear from the calculations that the most stable isomers of **4** are η^1-bound (the η^2-P_{basal}–P_{basal}-coordinated isomer **4G** has the highest relative energy of all calculated geometries). Therefore, we used mainly η^1-coordinated isomers as starting geometries for the larger and computationally more demanding $[Ag(P_4S_3)_3]^+$ **5** cations and omitted some less likely candidates. Here, the energetically most favored isomer **5E** has three Ag–P_{basal} coordinations (Figure 1), but again all other structures are not much higher in energy (four of the other calculated geometries are also found within $E_{rel.} \leq$ 16.9 kJ mol^{-1}). It should also be noted that the relative energies of those isomers in which the silver atom is six-coordinate (i.e., **5A** and **5C**) are thermodynamically less favorable. As further model compounds, different isomers of the $[Ag_2(P_4S_3)]^{2+}$ **6** dications were also assessed. Because η^3-coordinated species appeared to be unfavorable for the other calculated compounds, such isomers were omitted for this dication. As for the previous calculations, the relative ener-

gies of all calculated isomers of the model compounds **6** ($[Ag_2(P_4S_3)]^{2+}$) are all very similar (11 of 12 isomers within 22.9 kJ mol^{-1}).

From the preceding figures it is clear that the PES of the $[Ag_x(P_4S_3)_y]^{n+}$ ions is rather flat. This indicates that several different coordination modes in the $Ag(P_4S_3)$ complexes should be accessible in solution and may be even in the solid state, which is in agreement with the dynamic solution behavior reported.[18]

In most of the global minimum energy structures in Figure 1, η^1 coordination is favored, except for those in which the silver cations do not have access to other ligands which could saturate the positive charge, that is, in **3G**. These findings are in good agreement with the experimentally determined structures of the P_4S_3 adducts **1** and **2**, as well as those presented below, where only η^1-coordination has been observed.

Synthesis and solution NMR characterization: Reacting P_4S_3 with $[Ag(CH_2Cl_2)][hftb]$ or $Ag(CH_2Cl_2)_3[al\text{-}f\text{-}al]$ in CH_2Cl_2 or CH_2Cl_2/CS_2 mixtures at room temperature leads to the very air- and moisture-sensitive adducts $[(P_4S_3)Ag[hftb]]_\infty$ (**7**) [Eq. (1)]and $[Ag_2(P_4S_3)_6]^{2+}[al\text{-}f\text{-}al]^-_2$ (**8**) [Eq. (2)]. They are both highly soluble in CH_2Cl_2 and CH_2Cl_2/CS_2 mixtures.

$$[Ag(CH_2Cl_2)][hftb] + P_4S_3 \xrightarrow{CH_2Cl_2} [(P_4S_3)Ag[hftb]]\ \mathbf{7}\ (\text{yellow}) + CH_2Cl_2 \quad (1)$$

$$2[Ag(CH_2Cl_2)_3][al\text{-}f\text{-}al] + 6\,P_4S_3 \xrightarrow{CH_2Cl_2/C_2S_2} [Ag_2(P_4S_3)_6][al\text{-}f\text{-}al]_2\ \mathbf{8}\ (\text{colorless}) + 6\,CH_2Cl_2 \quad (2)$$

Initial in situ reactions in sealed NMR tubes with CD_2Cl_2 as a solvent, showed the same very simple ^{31}P signals as those found for $[(P_4S_3)Ag[hfip]]$ (**1**) and $[Ag(P_4S_3)_2][pftb]$ (**2**): One quartet and one doublet with shifts similar to free P_4S_3 in the same solvent ($\delta(^{31}P)(P_4S_3) = 73.1$ (q), -117.4 ppm (d)); in **7** and **8** the quartet of P_{apical} shifted by -6.9 and $+0.4$ ppm, the doublet of P_{basal} shifted by -10.8 and -0.7 ppm. This indicates that the bonding towards the Ag is only weak and that, in solution, exchange reactions take place. Even at temperatures as low as $-90\,^\circ C$, where pure P_4S_3 is insoluble in CH_2Cl_2, the spectra remained simple and unchanged. Coupling to $^{107/109}Ag$ could not be observed in any of the ^{31}P spectra. In a static system the multiplicity of these signals should change as the three P_{basal} atoms would not be chemically equivalent. Such changes were observed in more tightly bound complexes with other metals.[19] The ^{13}C, ^1H, and ^{27}Al NMR spectra showed that the anions remained intact during the reaction, however, the formation of adducts with weak cation–anion interactions and thus shifted anion resonances may be concluded for ***7*** (see $\Delta\delta$ and ω in Table 1).

For the model compounds **6A** and **6N** the calculated $\Delta\delta$ values do not fit very well to the signals observed in the ^{31}P NMR spectra in solution. This allows us to propose that such structures are absent in solutions of **7**. In the case of solutions of **8**, the calculated $\Delta\delta$ values of the $[Ag(P_4S_3)_3]^+$ ion **5E**, are very close to the observed shifts of **8** (much closer than those calculated for the $[Ag_2(P_4S_3)_6]^{2+}$ dication that was found in the solid state). This could be an indication that in solution the dication is not present. To investigate this hypothesis for **8**, an ESI MS in CH_2Cl_2 was recorded. In the cationic mode, signal groups for $[Ag(P_4S_3)_2]^+$ and $[Ag(P_4S_3)_3]^+$ are detected and, according to the mass distribution, no $[Ag_2(P_4S_3)_6]^{2+}$ is present in the solution. Possible reasons for this observation are discussed in a later section. In the negative mode, the $[al\text{-}f\text{-}al]^-$ ion (m/z 1483, 22%) and its further decomposition products are observed.

Solid-state ^{31}P NMR spectra: *Methodology*: In the weakly bound cationic complexes in **2**, **7**, and **8**, silver acts as a bridging atom between P_4S_3 cages, where the electrons of the molecular orbitals formed over the P-Ag-P bridge mediate dipole–dipole interactions between the phosphorus atoms (*J*-coupling). In solution, these two-bond $^2J_{P,Ag,P}$ couplings remain unobserved in NMR spectra of the $[Ag(P_4S_3)_n]^+$ complexes due to fast exchange between the P_4S_3 cages. In solids, such an exchange is unlikely. So if the $^2J_{P,Ag,P}$ couplings were observed they could provide more insight

Table 1. Comparison of the NMR shifts of **7** and **8** with those of the silver salts of $[hftb]^-$ and $[al\text{-}f\text{-}al]^-$, free P_4S_3 and the calculated shifts of P_4S_3, **6A**, **6N**, **5E**, and $[Ag_2(P_4S_3)_6]^{2+}$. All spectra were recorded at room temperature in CD_2Cl_2. Calculations at the (RI-)BP86 level of theory (basis sets: SVPallS2 for Ag atoms, SV(P) for P and S atoms). All values are given in ppm.

	7	Ag[hftb]	$\Delta\delta$ for **7**[a]	**8**	Ag[al-f-al]	$\Delta\delta$ for **8**[a]	P_4S_3	P_4S_3 calcd	$\Delta\delta_{calcd}$ for **6A**[b]	$\Delta\delta_{calcd}$ for **6N**[b]	$\Delta\delta_{calcd}$ for **5E**[b]	$\Delta\delta_{calcd}$ for $[Ag_2(P_4S_3)_6]^{2+}$[b]
$\delta(^1H)$	1.63, s	1.57, s	+0.05	–	–	–	–	–	–	–	–	–
$\delta(^{13}C)$	124.0, q	124.1, q	−0.1	121.0, q	121.0	0.0	–	–	–	–	–	–
	76.3, m	76.2, m	−0.1	78.4, m	78.7	−0.3	–	–	–	–	–	–
	18.0, s	17.9, s	+0.1	–	–	–	–	–	–	–	–	–
$\delta(^{31}P)$	−128.2, d	–	−10.8	−116.7, d	–	0.7	−117.4, d	−129.5	37.0	20.8	−15.7	−25.1
	66.2, q	–	−6.9	73.5, q	–	0.4	73.1, q	87.6	−35.5	−50.8	1.5	−40.0
$\delta(^{27}Al)$	47.2, s ($\omega_{1/2}$= 299 Hz)	47.1, s ($\omega_{1/2}$= 184 Hz)	+0.1	37.5, s ($\omega_{1/2}$= 3100 Hz)	33.5, s ($\omega_{1/2}$= 2200 Hz)	4.0	–	–	–	–	–	–

[a] $\Delta\delta = \delta(\text{adduct}) - \delta(\text{silver salt or } P_4S_3)$. [b] $\Delta\delta_{calcd} = \delta_{calcd}(\text{model compound}) - \delta_{calcd}(P_4S_3)$. For all P_{basal} and all P_{apical}, the average value of the calculated tensors has been used.

into a structure of these materials. To characterize solid Ag complexes we utilized the ^{31}P magic angle spinning (MAS) experiment,[21] along with two-dimensional (2D) ^{31}P *J*-resolved[22] and incredible natural abundance double-quantum transfer experiments (INADEQUATE).[23] These two-dimensional methods have first been proposed to study molecules in liquids and with some adaptations they have been successfully applied to characterize solids.

The INADEQUATE experiment was designed to study through-bond connectivities of molecules in solution by correlating resonances of the same nuclei between which *J* coupling exists. Few variants of this experiment have been proposed to study solids under MAS.[24,25] The complexes analyzed in this work show a degree of structural disorder so we used the double-quantum (DQ) refocused INADEQUATE MAS sequence as it offers an increased sensitivity.[25] An important question with this method is, if the observed correlation peaks are the result of excitation of the double-quantum transition exclusively through a *J*-coupling mechanism, which provides information on through-bond connectivities, or if they appear due to the through-space dipole–dipole interactions. This issue was elaborated in a recent paper by Fyon and co-workers in which it was demonstrated that the INADEQUATE MAS experiment is indeed a suitable probe of through-bond connectivities, although the interpretation of the obtained spectra should be taken with special care.[26] The 2D *J*-resolved MAS experiment was used to measure homonuclear ^{31}P *J* couplings.[27]

P_4S_3: The different modifications of P_4S_3 (α, β, and γ) have previously been studied in great detail by neutron diffraction and X-ray crystallography,[28,29] thermodynamic methods,[28,30] infrared and Raman spectroscopy,[31,32] and solid-state NMR spectroscopy.[33–36] It was found that the nearly spherical P_4S_3 molecules have a rigid structure,[28,29] whereas the entire molecules undergo reorientational jumps around the uniaxial threefold axis.[35,36] The rate of this motion at room temperature was estimated to be $k < 10^7\ s^{-1}$.[33] Chemical shift anisotropy (CSA) tensor parameters of the ^{31}P sites have been determined from the single crystal and MAS NMR spectra.[35,36] Due to fast reorientational motion each P_4S_3 molecule gives only one ^{31}P resonance for all P_{basal} sites at an averaged chemical shift and one resonance for P_{apical} atoms. The two P_{apical} atoms of the asymmetric unit cell experience the nonaveraged chemical shift anisotropy δ_{CSA} of 156 and 164 ppm, whereas the averaged δ_{CSA} for all P_{basal} atoms is about 277 ppm.[36] The through-space dipole–dipole coupling constant between pairs of $^{31}P_{basal}$–$^{31}P_{basal}$ in the absence of motion in a single P_4S_3 unit is about 1.7 kHz, taking into account the average distance of 224 pm. The plastic phase β-P_4S_3 is formed at 314 K through a first-order crystal-to-plastic phase transition. As the phase transition is approached the increase in librational amplitudes of P_4S_3 cages around the uniaxial threefold axis is predominant. Once the plastic phase is formed, the P_4S_3 cages undergo a fast pseudoisotropic motion in which the centers of gravity of P_4S_3 are well defined. The plastic β-form remains stable on cooling until 259 K when it is transformed back into the crystalline α-form.

Figure 2 shows the ^{31}P MAS NMR spectra of α-P_4S_3 (a) and β-P_4S_3 (b, c), whereas the ^{31}P isotropic chemical shifts (δ_{iso}) and the spin–lattice relaxation time constants (T_1) are

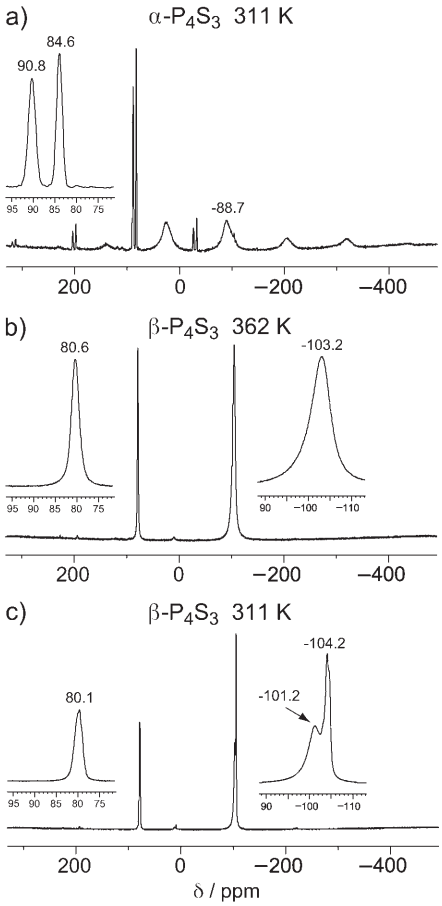

Figure 2. ^{31}P MAS NMR spectra of: a) α-, and b, c) β-P_4S_3 solids recorded at 311 K (a, c) and 362 K (b). The center bands are shown on an enlarged scale. Spectra are the result of averaging 8 transients with a recycle interval of 60 s.

listed in Tables 2 and 3, respectively. From the rotor-synchronized MAS spectra (not shown) the intensity ratios of $^{31}P_{apical}$:$^{31}P_{basal}$ resonances are estimated to be 1:3. The ^{31}P MAS spectrum of α-P_4S_3 exhibits an envelope of spinning

Table 2. Chemical shifts of ^{31}P resonances (δ_{iso} in ppm) in α-P_4S_3, β-P_4S_3 and the complexes **7**, **2**, and **8** measured at 311 K.

	α-P_4S_3	β-P_4S_3	**7**	**2**	**8**
$^{31}P_{apical}$(I)	90.8	80.1	67.5	86.3	87.3
$^{31}P_{apical}$(II)	84.6	80.1	63.8	81.0	73.3
$^{31}P_{apical}$(III)	–	–	–	79.9	72.3
$^{31}P_{apical}$(IV)	–	–	–	75.3	–
$^{31}P_{basal}$(I)	−88.7	−101.2	−134.1	−102.2	−106.6
$^{31}P_{basal}$(II)	−88.7	−104.2	−134.1	−105.8	−112.4
$^{31}P_{basal}$(III)	–	–	–	−107.7	−115.9
$^{31}P_{basal}$(IV)	–	–	–	−112.0	–

Table 3. Spin-lattice relaxation time constants T_1 [in s] of ^{31}P resonances in α-P_4S_3, β-P_4S_3, and the complexes **7**, **2**, and **8**. They were measured at 311 K by using inversion recovery experiment with a single π pulse used to invert the magnetization.

	α-P_4S_3	β-P_4S_3	**7**	**2**	**8**
$^{31}P_{apical}$(I)	67	2.6	2.5	0.91	1.7
$^{31}P_{apical}$(II)	67	2.6	2.7	1.0	1.1
$^{31}P_{apical}$(III)	–	–	–	1.7	1.1
$^{31}P_{apical}$(IV)	–	–	–	2.0	–
$^{31}P_{basal}$(I)	67	2.2	1.1	0.15	0.26
$^{31}P_{basal}$(II)	67	2.2	1.1	0.29	0.19
$^{31}P_{basal}$(III)	–	–	–	0.22	0.19
$^{31}P_{basal}$(IV)	–	–	–	0.39	–

sidebands covering approximately 100 kHz of spectral width. They are to be expected due to the large CSA interaction.[36] The linewidth (full-width-at-half-height) of $^{31}P_{apical}$(I) is 200 Hz and $^{31}P_{apical}$(II) is 250 Hz, whereas that of $^{31}P_{basal}$ (I, II) is ≈2.4 kHz. Distinctively larger linewidths of $^{31}P_{basal}$ atoms arise from the motional broadening that is the result of a combined effect of CSA interaction, MAS, and molecular motion.[37] Molecular reorientation of P_4S_3 around the uniaxial threefold axis only brings time averaging of the CSA interaction to $^{31}P_{basal}$ resonances, so the $^{31}P_{apical}$ resonances remain free from any motional broadening. This broadening is typically observed for the reorientational rates of $10^3\ s^{-1} < k < 10^8\ s^{-1}$. Barely any spinning sidebands are observed in the ^{31}P MAS NMR spectra (Figure 2b, c) of β-P_4S_3, which is not surprising because the P_4S_3 cages in the plastic phase undergo a fast pseudo-isotropic motion that completely averages the CSA interaction. Despite this random motion the P_4S_3 cages do have an averaged preferred orientation as evidenced by two nicely resolved $^{31}P_{basal}$ resonances in the spectrum recorded at 311 K (Figure 2). The possible existence of two inequivalent P_4S_3 units in β-P_4S_3 has been proposed in an earlier work of von Schnering and co-workers,[28,29] however, it is NMR spectroscopy that provides unambiguous evidence. It has been found that spin–lattice relaxation in both α- and β-P_4S_3 is dominated by the chemical shift anisotropy mechanism, whereas dipole–dipole interactions contribute to a lesser extent.[33] The much shorter relaxation times of ^{31}P in β-P_4S_3 in comparison to those of α-P_4S_3 are due to fast pseudoisotropic motion of the P_4S_3 cages which is estimated to be $k > 10^8\ s^{-1}$.[33]

$[Ag(P_4S_3)_2][pftb]$ ***2****, $[(P_4S_3)Ag(hftb)]$* ***7****, and $[Ag_2(P_4S_3)_6]^{2+}$ $[al\text{-}f\text{-}al]^-_2$* ***8***: Figure 3 shows ^{31}P MAS NMR spectra of **7**, **2**, and **8** recorded at 311 K. They all show an envelope of spinning sidebands spread over about 100 kHz indicating that the amplitudes of the ^{31}P CSA interactions are of the same order as those measured for α-P_4S_3. The linewidths of the spinning sidebands are remarkably narrow, typically about 200–300 Hz. In addition, the ^{31}P spin-lattice relaxation time constants (Table 3) are of the order of seconds or shorter. These observations indicate that the P_4S_3 cages undergo reorientational motions around the uniaxial threefold axis

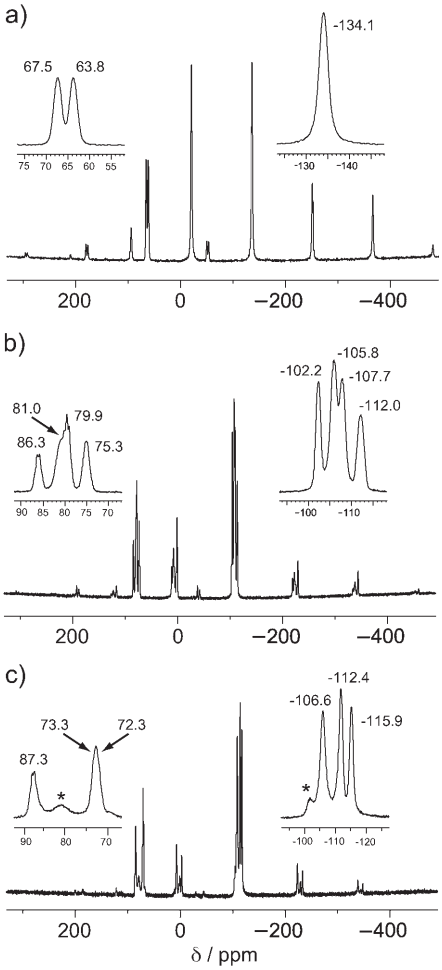

Figure 3. ^{31}P MAS NMR spectra of: a) **7**, b) **2**, and c) **8** recorded at 311 K. The center bands are shown on an enlarged scale. Spectra are the result of averaging 64 transients with a recycle interval of 10 s.

with a rate of $k > 10^8\ s^{-1}$. Spectra obtained with slower spinning rates (5 kHz) also exhibit narrow ^{31}P resonances suggesting that homonuclear dipole–dipole ^{31}P interactions, particularly those of the P_{basal} atoms, are significantly averaged by a fast molecular motion. However, scalar *J* couplings (either homonuclear or heteronuclear) remain unresolved except for a few of the $^{31}P_{apical}$ resonances of **2** and **8**, where poorly resolved $^2J_{P,S,P}$ couplings are evident. This is in contrast to the static adduct $(CuI)_3P_4S_4$ with longer relaxation times, where ^{31}P,^{63}Cu coupling is observed.[12] The asymmetric unit cell of **7** contains two P_4S_3 units resulting in two well-resolved $^{31}P_{apical}$ resonances (Figure 3a), but the $^{31}P_{basal}$ resonances of the two units have very similar averaged isotropic chemical shifts, so only a single resonance is observed. From the rotor-synchronized MAS spectra (Figure 4a, b) the relative intensity ratios of $^{31}P_{apical}$:$^{31}P_{basal}$ in all complexes studied here are estimated to be 1:3. Eight and six ^{31}P resonances in Figures 3b and 3c, respectively, correspond to the four and three different P_4S_3 cages of the asymmetric unit in **2** and **8**, respectively. In the temperature range 249–338 K, the ^{31}P MAS spectra of **2** reveal a slight chemical shift

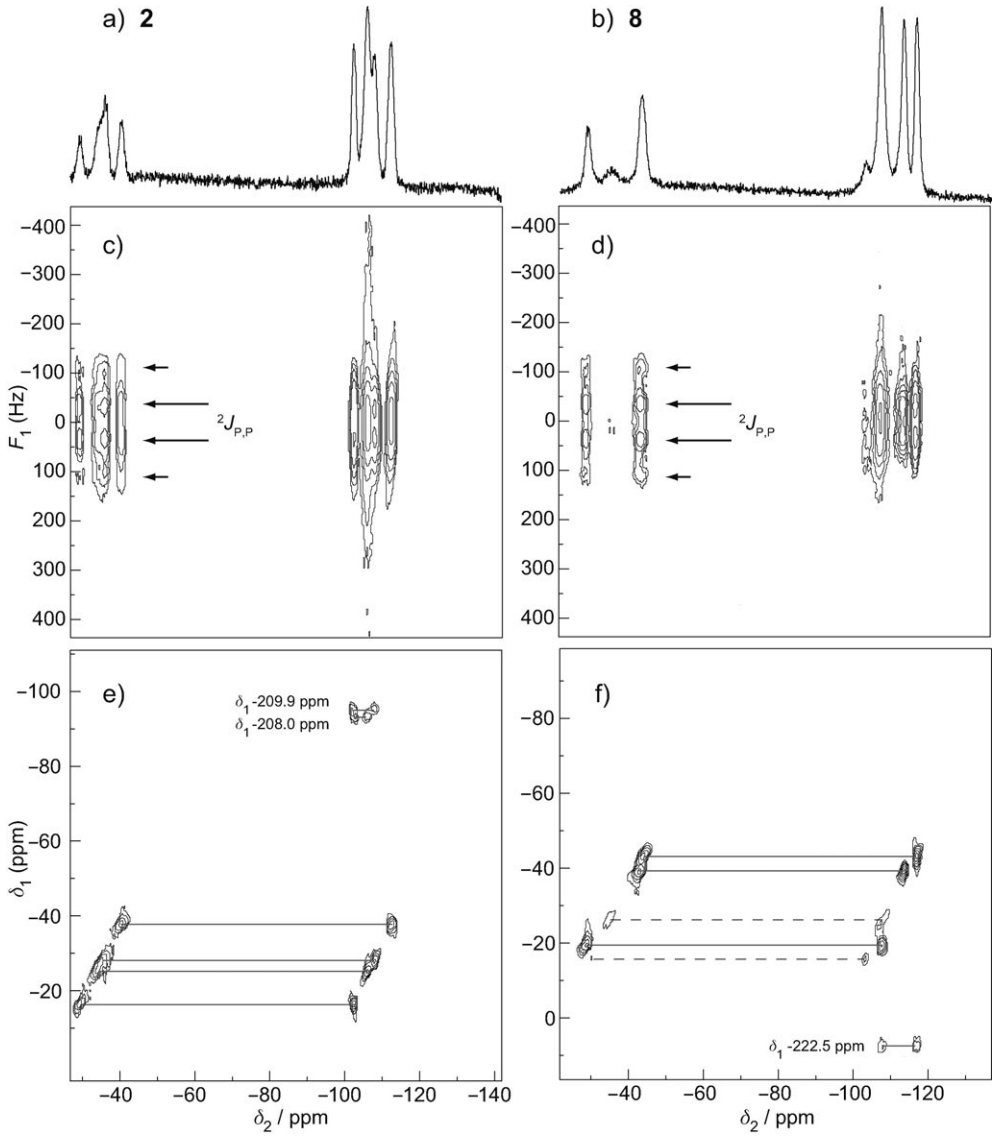

Figure 4. a, b) Rotor-synchronized ^{31}P MAS; c, d) ^{31}P *J*-resolved MAS and; e, f) ^{31}P INADEQUATE MAS spectra of **2** (a, c, and e) and **8** (b, d, and f). The spectra (a, b) are the result of averaging 8 transients with a recycle interval of 5 s. The two-dimensional spectra are the result of averaging 32 transients for each of 64 (c, d) and 156 (e, f) t_1 increments of 1.142 ms (c, d) and 71.4 μs (e, f), with a relaxation interval of 5 s. The excitation and reconversion intervals were 2.57 ms.

change (up to a few ppm) for all resonances, whereas only the $^{31}P_{basal}$(IV) resonance displays a dramatic increase in broadening at lower temperatures, suggesting slower reorientational motion for this P_4S_3(IV) cage, where $k < 10^7\ s^{-1}$. We find that the complexes **7** and **2** remain stable over a long period of time in a sealed container at room temperature, whereas the spectrum of complex **8** recorded after storage for a few days in the MAS container shows additional resonances with the same chemical shift and the same relaxation times of the ^{31}P resonances as α-P_4S_3. This is in agreement with DFT calculations, which showed that in the model system $[Ag(P_4S_3)_3]^+$ the third ligand is only very weakly bound. Similar energetics should also apply for the dication. After a few weeks the ^{31}P MAS spectrum of **8** was identical to that of α-P_4S_3. This observation confirms that complex **8** is metastable and one of its decomposition products is most likely to be the α-P_4S_3 phase.

The rotor-synchronized ^{31}P MAS, *J*-resolved MAS, and INADEQUATE MAS NMR spectra of **2** and **8** are shown in Figure 4. Due to rotor synchronization the $^{31}P_{apical}$ resonances are aliased in the direct dimension (δ_2) and the ppm scale is not reflecting their real chemical shifts. Similarly, in the indirect dimension (δ_1) of the INADEQUATE spectra all ^{31}P resonances are aliased and the scale is adjusted to reflect genuine shifts. For resonances where this was not possible, the isotropic chemical shifts are annotated on the spectrum. The projections of the ^{31}P resonances in the *J*-resolved spectra (Figure 4c, d) on to the δ_2 dimension reflect the homonuclear *J*-coupling multiples. Due to fast molecular motion the refocused linewidths of $^{31}P_{apical}$ resonances are re-

markably narrow (except for complex **7**, spectra not shown) and consequently the $^{31}P_{apical}$ quartets arising from $^{2}J_{P,S,P}$ are well resolved. For complex **2** we find the following values: $^{2}J_{P,S,P}(I) = 74$, $^{2}J_{P,S,P}(II) = 71$, $^{2}J_{P,S,P}(III) = 69$, and $^{2}J_{P,S,P}(IV) = 79$ Hz, and for **8**: $^{2}J_{P,S,P}(I) = 70$, $^{2}J_{P,S,P}(II) = 72$, and $^{2}J_{P,S,P}(III) = 72$ Hz. Similar values for $^{2}J_{P,S,P}$ couplings are measured in solutions. Somewhat larger refocused linewidths of $^{31}P_{basal}$ limit the resolution of these resonances. If $^{2}J_{P,Ag,P}$ couplings exist then these complex multiples are hidden behind what appears to be a broad $^{31}P_{basal}$ doublet structure. The 2D ^{31}P DQ INADEQUATE MAS NMR spectra in Figures 4e and f show correlation peaks for pairs of ^{31}P resonances between which *J* coupling exists. In the δ_1 dimension they are found at the sum of their chemical shifts. The INADEQUATE spectra allow the assignment of $^{31}P_{apical}$ and $^{31}P_{basal}$ resonances of the same cage (peaks at $-50\ ppm < \delta_1 < -20\ ppm$) as given in Tables 2 and 3, and to resolve peaks that are overlapped in the ^{31}P MAS spectra, for example, $P_{apical}(II)$ and $P_{apical}(III)$ of complexes **2** and **8**. More importantly, correlation peaks are also observed between phosphorus atoms of different P_4S_3 cages, providing direct evidence for the existence of $^{2}J_{P,Ag,P}$ couplings mediated through bridging Ag^+ ions. For complex **8** the correlation peaks at $\delta_1 = -222.5$ ppm (Figure 4f) are the consequence of a chemical bond between $P_{basal}(I)$–$P_{basal}(III)$ formed through the Ag^+ bridging cation. These are the only peaks expected to be seen because the other cages are linked through S atoms. Correlation peaks connected with dashed lines in the spectra are assigned to a small amount of unknown impurities or possible degradation products, even though spectra were recorded immediately after the sample preparation. Only two sets of correlation peaks at δ_1 of -209.9 and -208.0 ppm are observed for complex **2** suggesting a correlation between $P_{basal}(I)$–$P_{basal}(II)$ and $P_{basal}(I)$–$P_{basal}(III)$. This is surprising because the cluster arrangement in this compound should result in a total of six pairs of peaks. As the refocused linewidths are of the same order for all $^{31}P_{basal}$ resonances, the most likely explanation for the missing peaks is that all other $^{2}J_{P,Ag,P}$ couplings are considerably smaller.

Crystal structures: *Redetermination of the structures of α- and γ-P_4S_3*: The structures of α- and γ-P_4S_3 were redetermined at 140 K to compare the solid-state structure of the adducts with that of the free ligand under similar conditions; both data sets also have a better quality ($R1 = 1.73\%$ for γ-P_4S_3 and 2.77% for α-P_4S_3) than those reported before.[11,29,38] More detailed information on the solid-state structures can be found in the Supporting Information. A comparison of the bond lengths is listed in Table 4.

[Ag(P₄S₃)₂][pftb] ***2***: The ^{31}P solid-state NMR measurements on this compound during this study clearly showed that the previously published space group $P2_1/n$[18] was not correct. Therefore, we redetermined the crystal structure in $P2_1$, in which the number of the symmetrically independent P_4S_3 moieties is doubled if compared to $P2_1/n$. Because the bond lengths and angles did not change significantly, the structural parameters are not discussed in the main text of this publication (a detailed figure of the redetermined solid-state structure of **2** is shown in the Supporting Information).

[(P₄S₃)Ag[hftb]]₈ ***7***: Complex **7** crystallizes in the triclinic space group $P1$ with $Z = 2$. A section of the solid-state structure is shown in Figure 5. Although it is also possible to solve the structure as monoclinic in the space group $P2_1$, solid-state ^{31}P NMR clearly reveals that there are two independent P_4S_3 moieties in the asymmetric unit. As it can be seen from Figure 5 and Table 4 in which the characteristic bond lengths of **7** are listed, the two parts of the asymmetric units differ only very slightly, but these small changes are enough to give rise to different peaks in the solid-state NMR. This adduct forms one-dimensional polymeric chains. In these chains, the Ag^+ ion is coordinated by one apical and one basal P atom of the P_4S_3 cages. Additionally, two oxygen atoms of the anion are also coordinated to the silver atom, which leads to a molecular species with the same structural pattern as in the side form of the $[(P_4S_3)Ag[hfip]]_\infty$ (**1**).[18] The structural parameters of the anion are normal.[17] The Ag–P distances are 245.67(8)/246.09(7) and 254.76(8)/254.64(8) pm and (P_{apical} and P_{basal}, respectively); the Ag–O bonds are 241.85(11)/241.72(12) and 239.36(11)/

Table 4. Comparison of selected bond lengths of **2** at 150 K, **7** at 100 K, **8** at 130 K, and P_4S_3 (α and γ modification) at 140 K.

	2 (150 K)	**7** (100 K)	**8** (130 K)	γ-P_4S_3 (140 K)	α-P_4S_3 (140 K)
d(Ag–O) [pm]	–	239.2(1)–241.9(1) av 240.5	–	–	–
d(Ag–P_{basal}) [pm]	250.9(3)–254.9(3) av 253.2	254.6(1)–254.8(1) av 254.7	258.8(2) (bridging) 248.3(2) (terminal)	–	–
d(Ag–P_{apical}) [pm]	–	245.7(1)–246.1(1) av 245.9	–	–	–
d(Ag–S) [pm]	265.5(3)–265.6(3) av 265.6	–	262.5(2) (bridging) 263.4(2) (terminal)	–	–
d(P_{basal}–P_{basal}) [pm]	222.1(4)–226.2(5) 224.1	222.9(1)–225.2(1) av 223.9	221.3(2)–224.8(2) av 223.0	223.6(1)–224.5(1) av 224.2	223.7(1)–224.8(1) av 224.1
d(P_{basal}–S) [pm]	206.6(4)–210.2(5) av 208.0	209.0(1)–210.9(1) av 209.9	206.9(2)–211.3(2) av 209.0	209.6(1)–210.7(1) av 209.9	210.6(1)–210.9(1) av 210.7
d(P_{apical}–S) [pm]	210.1(5)–213.8(4) av 211.2	208.5(1)–209.7(1) 209.1	209.0(2)–213.5(2) av 210.6	210.4(1)–211.4(1) av 211.0	210.6(1)

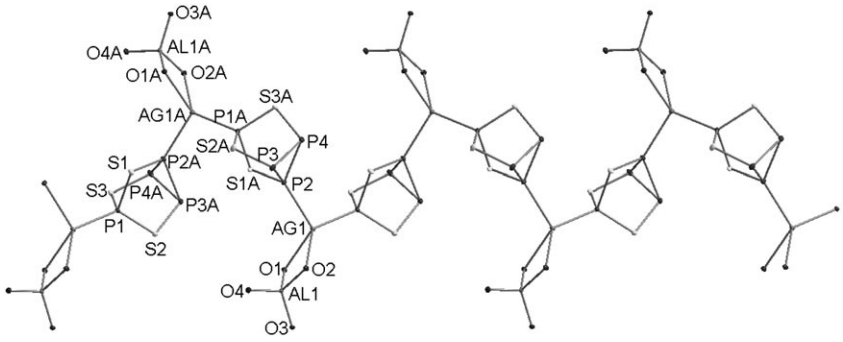

Figure 5. Section of the polymeric chain of $[(P_4S_3)Ag[hftb]]$ **7** in the solid state at 100 K; thermal displacement ellipsoids showing 25% probability. The $C(CH_3)(CF_3)_2$ groups have been omitted for clarity.

239.19(11) pm. These values differ from those of the (disordered) side form of $[(P_4S_3)Ag[hfip]]$ by up to 17.5 pm (d(Ag–P_{apical}) 228.5(3), d(Ag–P_{basal}) 249.7(7) pm).[18] However, these differences should be attributed to the inherent disorder in $[(P_4S_3)Ag[hfip]]$, and the structure of **7** should be used as a reference for the structural parameters of such a structural motif.

X-ray diffraction at 283 K shows essentially the same structure with larger thermal displacement parameters (tdps) for the CF_3 groups of the anion; the tdp for the Ag and the P_4S_3 moieties remain very small and almost spherical (see the Supporting Information). This implies that on the timescale of X-ray scattering the structure is static and any dynamics, except rotation about the CF_3 groups, has to be short lived with no long-lived resting state that may add to the diffraction pattern as a second orientation. A similar conclusion was drawn from an analysis of the Raman and IR spectrum of **7** (see below).

$[Ag_2(P_4S_3)_6]^{2+}[al\text{-}f\text{-}al]^-_2$ ***8***: Complex **8** crystallizes in the monoclinic space group $P2_1$ with $Z=2$. The solid-state structure of the cation at 130 K is shown in Figure 6, a picture including both anions is given in the Supporting Information.

Complex **8** is an ordered AB_2 salt with isolated C_i-symmetric $[Ag_2(P_4S_3)_6]^{2+}$ dications A and [al-f-al]$^-$ anions B. In the centrosymmetric dications, only η^1 coordination of the P_4S_3 cages towards the silver atoms is observed. The two bridging ligands coordinate with one basal P atom and one S atom; the terminal ligands coordinate only with one P_{basal} or one S atom to Ag atoms. The structural parameters of the anion are normal.[39] However, in contrast to other salts, the Al-F-Al bridge in **8** is not linear (172.4(2)°). This is probably due to packing effects in the crystals. The cation–anion interactions are very weak (4 Ag–S and 14 Ag–P contacts between 311.6 (P)/320.0 (S) and 336.4 (P)/323.5 pm (S), average value: 327.0 (P)/322.8 pm (S)). No Ag–F contacts below the sum of the van der Waals radii of 320 pm could be observed. Because only S5/S5a show weak contacts towards the fluorine atoms, but ten P atoms have contacts to the F atoms it appears reasonable to argue that the phosphorus atoms are more positively charged than the sulfur atoms. In the solid state, these dications form stacked structures (see the Supporting Information).

In the complexes **2**, **7**, and **8**, the bond lengths of the P_4S_3 moieties do not change very much when compared to those of free P_4S_3, again, indicative of weak coordination.

Complex **8** contains an eight-membered folded ring that was first observed in the structure of $[Ag(P_4S_3)_2][pftb]$ (Figure 7).[18] The structural parameters of both rings are similar and agree within a few pm and a few degrees. The bond lengths and angles of both compounds, as well as the computed values for a C_i-symmetric $[Ag_2(P_4S_3)_6]^{2+}$ dication, are compared in the Supporting Information.

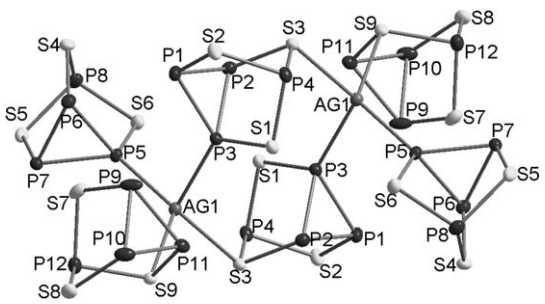

Figure 6. Solid-state structure of the $[Ag_2(P_4S_3)_6]^{2+}$ dication in **8** at 130 K; thermal displacement ellipsoids showing 25% probability.

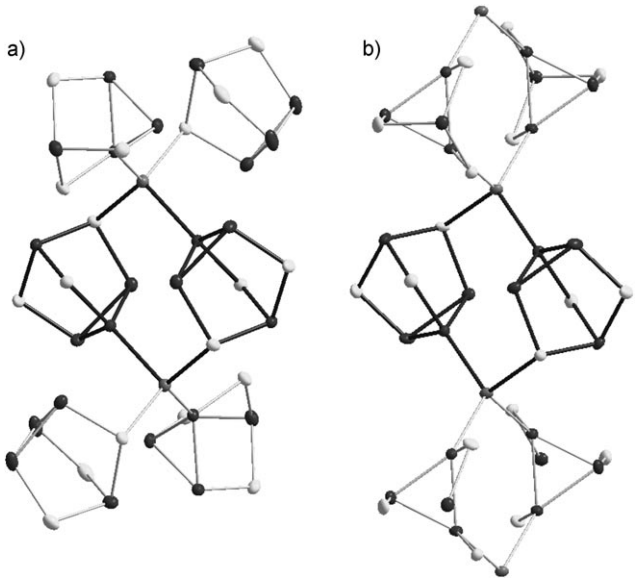

Figure 7. Relation between the cationic structures of the polymeric cation in $[Ag(P_4S_3)_2][pftb]$ **2**[18] (a, left) and the isolated dication in **8** (b, right).

Not only the cationic structures show similarities, but also the packing diagrams of both compounds are related. The packing of both substances is determined by the cations, which are aligned along the crystallographic *b* axis (packing diagrams of both compounds are given in the Supporting Information). The anions are placed in the space between the polymeric chains (for $[Ag(P_4S_3)_2][pftb]$ **2**) or the stacked dications (in the case of **8**). As the [al-f-al]$^-$ ions are much larger than [pftb]$^-$ they "break" the cationic chain, and the resulting free coordination sites are filled by additional P_4S_3 molecules. Overall, this effect may lead to the formation of the dications (Figure 7).

Born–Haber cycle investigation on the existence of the $[Ag_2(P_4S_3)_6]^{2+}$ dication in all phases: To answer the question of why the $[Ag_2(P_4S_3)_6]^{2+}$ dication was found in the solid state, but $[Ag(P_4S_3)_3]^+$ monocations were found in solution (as suggested by ESI mass spectrometry and NMR shift calculations) a suitable Born–Haber cycle has been established. The lattice enthalpies of both salts were calculated by using volume-based thermodynamics (VBT)[40] methods base on the molecular volumes of 3.30 and 1.65 nm^3 for **8** and $[Ag(P_4S_3)_3][al\text{-}f\text{-}al]$, respectively, (Scheme 1). Gas phase and solution free energies stem from BP86/SV(P) calculations including the COSMO solvation model (CH_2Cl_2 as solvent) as well as thermal and entropic contributions to the Gibbs energy at 195 and 298 K.

The formation of two $[Ag(P_4S_3)_3]^+$ monocations is thermodynamically favored in the gas phase and in solution (Coulomb explosion), whereas in the solid state, the higher lattice enthalpy of the 2:1 salt **8** leads to a stabilization of the dicationic form. Analogous Coulomb explosions have been reported for the cation pair $S_4^{2+}/2\ S_2^+$; $S_3N_2^{2+}/SN^+$ and S_2N^+ and others.[4,41]

IR and Raman spectra: In the Raman and IR spectra of **7** the bands of the $Ag(P_4S_3)$ moieties are observed between 117 and 495 cm^{-1}. These frequencies fit very well with those assigned to the side isomer of $[(P_4S_3)Ag[hfip]]$[18] and with those obtained by simulating the vibrational spectrum of the $[Ag_2(P_4S_3)]^{2+}$ dication and isomer **6A** in Figure 1. Compared to other P_4S_3 complexes (e.g., $(P_4S_3)(BX_3)$ (X: Br, I)[8]) the energy of the highest bands (e symmetry, at 488/9 cm^{-1}) remain nearly unchanged if compared to the free P_4S_3 (see Table 5). In case of a stronger coordination of the ligand, the energy of this vibrational band should be lowered. In our complexes, due to the very weak coordination, the interaction between the Ag^+ and the P_4S_3 cages leads to a slightly disturbed symmetry, whereas the bonding in the ligands

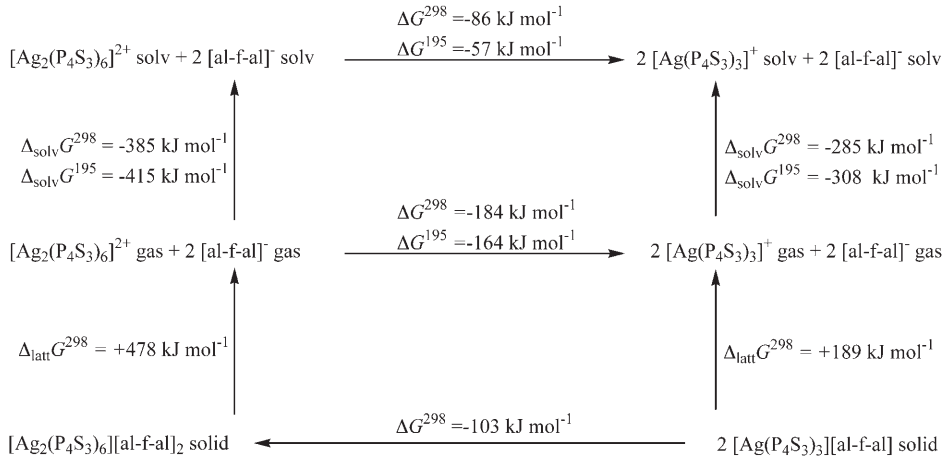

Scheme 1. Born–Haber cycle investigations of **8**. Values at the (RI)-BP86/SV(P) level of theory. The lattice free energies $\Delta_{latt}G$ were calculated by using VBT[40] and the solvation free energies $\Delta_{solv}G$ by the COSMO model.

Table 5. Comparison of the vibrational frequencies [cm^{-1}] of $[(P_4S_3)Ag[hftb]]$ (**7**) and $[Ag_2(P_4S_3)_6]^{2+}[al\text{-}f\text{-}al]_2^-$ (**8**) (bands of the anions have been omitted for clarity) with $[(P_4S_3)Ag[hfip]]$ (**1**), free P_4S_3, the calculated frequencies for the two possible isomers **6D** and **6A** of the $[Ag_2(P_4S_3)]^{2+}$ fragments and for the $[Ag_2(P_4S_3)_6]^{2+}$ dication. Calculations are at the (RI)-BP86/SV(P) level of theory. Raman intensities are given in %; IR intensities are given as follows: w: weak, mw: medium weak, m: medium, ms: medium strong, s: strong, vs: very strong.

P_4S_3 exptl Raman	P_4S_3 exptl IR[a]	P_4S_3 calcd IR (Sym)[b]	**7** exptl Raman	**7** exptl IR	isomer **6A** calcd IR	**8** exptl Raman	**8** exptl IR	$[Ag_2(P_4S_3)_6]^{2+}$ calcd IR
489	488(m)	463 E	498(15%)	495(mw))	492	493(38%)	491(w)	484, 469
–	–		470(100%)	485(mw)	478	468(50%)	–	–
–	–	447 A_1	–	–	457	447(100%)	–	457, 442
443	438(vs)	428 A_1	444(18%)	–	437	432(38%)	430(ms)	427
–	–	–	–	–	410 (2×)	415(24%)	409(m)	418
422	414(s)	387 A_1	–	394(ms)	400	–	–	400
–	–	389 E	–	–	–	–	377(ms)	382, 367
–	–	–	364(25%)	363(w)	–	–	–	–
–	–	–	352(49%)	351(w)	357	–	–	355
–	–	–	–	–	–	–	–	–
343	339(w)	323 E	–	338(mw)	334	346(86%)	347(w)	343
–	–	–	–	–	–	325(26%)	318(mw)	316
286	286(m)	287 E	299(30%), 289(37%)	298(ms)	285, 267	289(64%)	288(m)	289
–	–	–	–	–	–	246(24%)	–	247
221	218(s)	219 E	224(39%)	–	214, 209	222(40%)	–	226
187	184(s)	190 A_2	198(3%)	–	177	193(8%)	–	214
–	–	–	117(8%)	–	127	–	–	112

[a] See reference [31]. [b] See reference [18].

remains almost unchanged. A similar observation has been made for the $[Ag(P_4)_2]^+$ ion.[5]

Conclusions

Although the fluorinated silver alkoxy aluminates used in this study are very similar, their P_4S_3 adducts are not. In Table 6, some properties of these compounds are summarized. For the smaller and more basic anions $[hfip]^-$ and $[hftb]^-$, polymeric molecular structures are obtained, in which the Ag^+ ion is coordinated by P_4S_3 and by two alkoxy groups from the anion. In the case of the less basic $[pftb]^-$, the anion does not coordinate the silver cation and polymeric $[Ag(P_4S_3)_2]_8$ cations are formed. For the largest and least basic $[al\text{-}f\text{-}al]^-$ ion, the adduct is dicationic with well-separated dications and monoanions. However, even the large $[al\text{-}f\text{-}al]^-$ ion is too small to allow preparation of a simple isolated $[Ag(P_4S_3)_n]^+$ monocation, instead dimerization in the solid state with formation of the lattice-stabilized dimeric $[Ag_2(P_4S_3)_6]^{2+}$ dication is seen. This $[Ag_2(P_4S_3)_6][al\text{-}f\text{-}al]_2$ salt **8** is the first 2:1 salt of this fluorine-bridged $[al\text{-}f\text{-}al]^-$ anion. As shown by ESI-MS, DFT, and Born–Haber cycle calculations, this dication is unstable in the gas phase and in solution ("Coulomb explosion") [Eq. (3)].

Table 6. Comparison of the $Ag(P_4S_3)$ adducts of the $[hfip]^-$, $[hftb]^-$, $[pftb]^-$, and $[al\text{-}f\text{-}al]^-$ ion.

	$[hfip]^-$ **1**[a]	$[hftb]^-$ **7**	$[pftb]^-$ **2**[a]	$[al\text{-}f\text{-}al]^-$ **8**
basicity of the anion	low	lower		lowest
volume of the anion [nm^3]	0.599[b]	0.663[d]	0.758[b]	1.113[d]
P_4S_3 per Ag	1	1	2	3
coordination towards Ag	1 P_{apical}, 1 P_{basal},2 O[e]	1 P_{basal}, 1 S,2 O	3 P_{basal}, 1 S	2 P_{basal}, 2 S
$\delta(^{31}P)$ in CD_2Cl_2 [ppm]	+67 (q) −126 (d)	+67 (q) −128 (d)	+72 (q) −118 (d)	+73 (q) −117 (d)
av d(P–S) [pm]	216_{apical}, 207_{basal}[f]	209_{apical}, 208_{basal}	211_{apical}, 208_{basal}	211_{apical}, 209_{basal}
av d(P–P) [pm]	226	223	224	223
cation structure	polymeric	polymeric	polymeric	dimeric
structure of the adduct	molecular	molecular	ionic	ionic

[a] See reference [18]. [b] See reference [42]. [c] Determined by using the thermochemical volume of the $[hfip]^-$ ion[42] and the crystal structures of **1** and **7**. [d] Determined by using the thermochemical volume of the $[pftb]^-$ ion[42] and the crystal structures of $[CI_3][pftb]$[43] and $[CI_3][al\text{-}f\text{-}al]$.[44] [e] Main form; side form: 1 P_{basal}, 1 S, 2 O. [f] Disordered structure, less accurate.

$$2\,[Ag(P_4S_3)_3] + (\mathbf{5E}) \underset{\text{gas-phase solution}}{\overset{\text{solid state}}{\rightleftharpoons}} [Ag_2(P_4S_3)_6]^{2+} \qquad (3)$$

According to the BHC in Scheme 1 a weakly coordinating anion $[A]^-$ of approximately 3.8 nm^3 would be needed to stabilize a monomeric $[Ag(P_4S_3)_3]^+[A]^-$ salt. This should be contrasted with the volume of $[al\text{-}f\text{-}al]^-$ of 1.113 nm^3. Currently no well-defined WCA with a volume as large as 3.8 nm^3 is known. From Table 6 one can also see that with larger and less basic anions more P_4S_3 cages can be coordinated. In all of these adducts, only η^1 coordination is observed, which is in agreement with the calculation of the model compounds, which only predict an η^2-coordinated global minimum for $[Ag(P_4S_3)]^+$ **3**. In this case the η^2 coordination is probably due to the fact that there are no other molecules which could coordinate to the silver cation. In all other assessed cases η^1 coordination is preferred.

In solution, the NMR shifts of all adducts remain nearly unchanged if compared to the free ligand, which indicates dynamics and fast exchange processes. However, for **8** the ESI-MS and also the calculated $\Delta\delta(^{31}P)$ NMR values indicate the presence of the $[Ag(P_4S_3)_3]^+$ ion in solution, whereas in the solid state the dication $[Ag_2(P_4S_3)_6]^{2+}$ is favored (Scheme 1). Thus, the dynamics are likely to be due to exchanging $Ag(P_4S_3)_x^+$ structures and not due to exchange with the solvent CH_2Cl_2. The same conclusion can be drawn from the solid-state ^{31}P NMR spectra, which clearly reveal that these systems are, in contrast to the related, but static compound $(CuI)_3P_4S_4$,[12] very dynamic, even at low temperature, although the low- and ambient-temperature X-ray diffraction measurements of the $Ag(P_4S_3)$ complexes investigated in this study suggest rigid structures. As X-ray crystallography is an average method, this notion implies that the resting states for the dynamics observed by MAS-NMR spectroscopy are long-lived. Those conformations, which are intermediates for the dynamic exchange are very short lived and do not contribute, as "disorder", to the intensity data of the crystal structure determination. These conclusions are also in agreement with the flat calculated PES values of the various $[Ag(P_4S_3)_n]^+$ isomers with $n=1$, 2, 3. These flat PESs, and the fact that both S and P coordination is observed in the solid-state structures, also indicates that degradation can occur both through sulfidic and phosphidic pathways.

Experimental Section

Sample preparation: All manipulations were performed by using grease-free Schlenk or dry-box techniques and a dinitrogen or argon atmosphere (H_2O and $O_2<1$ ppm). Apparatus was closed by J. Young valves. The solvents were rigorously dried over P_2O_5, distilled, and degassed prior to use and were stored under N_2 on molecular sieves (4 Å). $Ag(CH_2Cl_2)$-[hftb],[17] Li[hfip],[17] Ag[hfip],[17] $[Ag(CH_2Cl_2)_3][al\text{-}f\text{-}al]$,[39] $[(P_4S_3)Ag[hfip]$ **1**,[18] and $[Ag(P_4S_3)_2][pftb]]$ **2**[18] were prepared as previously described. P_4S_3 was purified by extraction with CS_2. Crystals were grown from highly concentrated, oily solutions at room temperature or in a freezer (at −25 °C) because all adducts were highly soluble in CH_2Cl_2 and CH_2Cl_2/CS_2 mixtures.

NMR spectroscopy: NMR spectra (in CD_2Cl_2) were recorded by using a Bruker AC250 and by using a Bruker AVANCE 400 spectrometer and were referenced against the solvent (^1H, ^{13}C) or external aqueous $AlCl_3$ (^{27}Al) and 85 % H_3PO_4 (^{31}P). Solid-state ^{31}P NMR spectra were recorded on a Bruker DRX 300 spectrometer equipped with 7.0 T wide-bore magnet, and with a 4 mm CPMAS probe head. Well-powdered samples were packed under N_2 atmosphere into ZrO_2 rotors (with 4-mm outer diameter) and the magic-angle sample spinning was used at the rate of

14 kHz. Two-dimensional refocused INADEQUATE MAS spectra were recorded with rotor synchronization of the halves of the excitation and reconversion periods, the t_1 evolution period, and the acquisition period. The *J*-resolved spectra were recorded with rotor synchronization of the acquisition period and the halves of t_1 evolution period. Chemical shifts of ^{31}P are reported in ppm relative to an external 85 % H_3PO_4(aq) standard. The absolute temperature was calibrated from the chemical shift difference of the proton resonances in liquid methanol that was spun up to 14 kHz in order to account for frictional heating of 14 K (RT 297 + 14 K = 311 K).[45]

Vibrational and mass spectrometry: Raman spectra were recorded at room temperature on a Bruker RAM II FT Raman spectrometer (by using a liquid-nitrogen-cooled, highly sensitive Ge detector) in sealed NMR tubes or melting-point capillaries (1064 nm radiation, 2 cm^{-1} resolution). IR spectra of samples in Nujol mull between CsI or AgBr plates were recorded on a Bruker VERTEX 70 and a Bruker IFS 66v spectrometer. UV/Vis spectra were recorded on samples in Nujol mull between quartz plates on a Perkin–Elmer Lambda 900. The ESI mass spectra of **8** were measured by using a Q-TOF ULTIMA mass spectrometer (MICROMASS, Manchester, UK) equipped with a Z-spray-type ESI source. Phosphoric acid was used for the negative ion mass calibration range of 100–2000 *m*/*z*. Data were acquired and processed by using MASSLYNX version 4.0. Electrospray conditions were as follows: capillary voltage, 3 kV; source temperature, 80 °C; cone voltage, 35 V; and source block temperature, 150 °C. Nitrogen gas was used for ESI nebulization and drying. The sample was introduced through a syringe pump operating at 10 mL min^{-1}.

X-ray diffraction crystal-structure determination: Data collection for X-ray structure determinations was performed by using a STOE IPDS II, an Oxford Diffraction SAPHIRE/KM4 CCD (kappa geometry) and a Bruker APEX II diffractometer, all with graphite-monochromated $Mo_{K\alpha}$ (0.71073 Å) radiation. Single crystals were mounted in perfluoroether oil on top of a glass fiber, which was then brought into the cold stream of a low-temperature device so that the oil solidified. All calculations were performed on PCs equipped with the SHELXTL software package. The structures were solved by the Patterson heavy atom method or direct methods and successive interpretation of the difference Fourier maps, followed by least-squares refinement. All non-hydrogen atoms were refined anisotropically. The hydrogen atoms were included in the refinement in calculated positions by a riding model by using fixed isotropic parameters. Details of the refinement are collected in Table 7. Pictures of the measured structures were created with the program Diamond 3.1.

[(P_4S_3)Ag[hftb]] (7): Solid $Ag(CH_2Cl_2)$[hftb] (0.301 g, 0.32 mmol) and solid P_4S_3 (0.070 g, 0.32 mmol) were weighed into a specially designed Schlenk vessel (see Supporting Information). CH_2Cl_2 (5 mL) was added at room temperature and the mixture was stirred for 2 h after which a yellow solution over a smaller amount of dark brownish precipitate had formed. The suspension was filtered through a G4 frit plate, the filtrate was concentrated to a high degree and stored overnight at room temperature. Large yellow, very air- and moisture-sensitive needles of [(P_4S_3)Ag[hftb]] formed. Yield: 0.312 g, 90.6 %; ^1H NMR (250 MHz, CD_2Cl_2, 300 K): $\delta = 1.63$ ppm (s); ^{13}C NMR (63 MHz, CD_2Cl_2, 300 K): $\delta = 124.0$ (q, $^1J_{C,F} = 288.1$ Hz), 76.3 (m), 18.0 ppm (s); ^{19}F NMR (235 MHz CD_2Cl_2, 300 K): $\delta = -78.6$ ppm (s); ^{27}Al NMR (78 MHz, CD_2Cl_2, 300 K): $\delta = 47.2$ ppm (s br, $\omega_{1/2} = 299$ Hz); ^{31}P NMR (101 MHz, CD_2Cl_2, 300 K): $\delta = 66.2$ (q, $^2J_{P,P} = 61.8$ Hz), −128.2 ppm (d, $^2J_{P,P} = 61.9$ Hz); IR (AgBr plates, Nujol mull): $\tilde{\nu} = 298$ (ms), 328 (mw), 338 (mw), 351 (w), 363 (w), 394 (ms), 438 (ms), 462 (w), 485 (mw), 495 (mw), 535 (ms) 573 (ms), 619 (ms), 628 (ms), 669 (w), 700 (s), 728 (vs), 770 (ms), 794 (s), 865 (s), 890 (w), 974 (s), 1016 (w), 1079 (m), 1089 (m), 1112 (ms), 1175 (ms), 1169 (ms), 1225 (ms), 1241 (m), 1262 (m), 1303 cm^{-1} (ms); Raman: $\tilde{\nu} = 117$, 198, 223, 290, 299, 353, 365, 444, 470, 498, 536, 567, 697, 705, 773 cm^{-1}; UV/Vis (Nujol mull): $\lambda_{max} = 246$, 340, 402 nm.

[$Ag_2(P_4S_3)_6$][al-f-al]$_2$ (8): Solid [$Ag(CH_2Cl_2)_3$][al-f-al] (0.491 g, 0.26 mmol) and solid P_4S_3 (0.266 g, 0.78 mmol) were weighed into a specially designed Schlenk vessel (see the Supporting Information). CS_2 (2 mL) and CH_2Cl_2 (15 mL) were added at room temperature and the mixture was stirred overnight after which a colorless solution over a smaller amount of dark brownish precipitate had formed. The suspension was filtered through a G4 frit plate, the filtrate was concentrated and stored over-

Table 7. Crystallographic details of the two modifications of P_4S_3 at 140 K, **2** at 150 K, **7** at 100 K and 283 K, and **8** at 130 K.

	γ-P_4S_3 (140 K)	α-P_4S_3 (140 K)	**2** (150 K)	**7** (100 K)	**7** (283 K)	**8** (130 K)
crystal size [mm]	0.2 × 0.2 × 0.2	0.2 × 0.2 × 0.2	0.3 × 0.3 × 0.4	0.4 × 0.4 × 0.4	0.3 × 0.3 × 0.2	0.5 × 0.08 × 0.08
crystal system	orthorhombic	orthorhombic	monoclinic	triclinic	triclinic	monoclinic
space group	*Pnma*	*Pnma*	$P2_1$	$P\bar{1}$	$P\bar{1}$	$P2_1$
a [pm]	10.8734(10)	10.4738(7)	16.360(3)	10.547(2)	10.656(2)	1751.8(4)
b [pm]	9.7634(9)	9.5861(7)	10.954(2)	11.443(2)	11.596(2)	1254.8(3)
c [pm]	6.4321(6)	13.6715(10)	26.516(5)	14.459(3)	14.477(3)	3004.6(6)
α [°]	90	90	90	89.94(3)	89.96(3)	90
β [°]	90	90	94.66(3)	83.50(3)	83.40(3)	91.26(3)
γ [°]	90	90	90	89.90(3)	89.90(3)	90
V [nm^3]	682.84(11)	1372.66(17)	4736.1(16)	1733.7(6)	1777.1(6)	6.603(2)
Z	4	8	2	2	2	2
ρ_{calcd} [Mg m^{-3}]	2.141	2.130	2.232	2.067	2.017	2.625
μ [mm^{-1}]	1.896	1.886	1.242	1.128	1.101	1.104
abs correction	empirical	empirical	numerical	empirical	empirical	numerical
F(000)	432	864	3064	1048	1048	4336
index range	*h*: −14 to 14	*h*: −13 to 13	*h*: −13 to 20	*h*: −13 to 13	*h*: −16 to 16	*h*: −21 to 21
	k: −11 to 10	*k*: −12 to 13	*k*: −13 to 12	*k*: −14 to 14	*k*: −14 to 18	*k*: −15 to 10
	l: −8 to 8	*l*: −18 to 18	*l*: −32 to 31	*l*: −18 to 18	*l*: −21 to 21	*l*: −35 to 36
max 2θ	58.32	58.38	51.96	54.00	69.22	52.06
T [K]	140	140	150	100	283	130
diffractometer type	Oxford KM4/CCD	Oxford KM4/CCD	Stoe IPDS II	Bruker Apex II	Bruker Apex II	Stoe IPDS II
unique reflns [$I > 2\sigma(I)$]	854	1800	13100	15640	17701	11686
data/restraints/parameters	854/0/37	1800/0/73	13100/235/1788	15640/3/957	17701/3/957	11686/0/982
GOOF	0.946	1.071	1.042	1.147	1.018	0.973
final *R*1 [$I > 2\sigma(I)$]	0.0173	0.0278	0.0299	0.0165	0.0570	0.0542
final *wR*2	0.0439	0.0682	0.0775	0.0441	0.165	0.1345
largest residual peak [e $Å^{-3}$]	0.252	0.556	0.559	0.448	1.676	0.855
largest residual hole [e $Å^{-3}$]	−0.291	−0.322	−0.474	−0.342	−0.786	−0.673

night in a freezer (at −25 °C). Large colorless, very air- and moisture-sensitive needles of $[Ag_2(P_4S_3)_6][al\text{-}f\text{-}al]_2$ formed. Yield: 0.442 g, 90.1 %; ^{13}C NMR (63 MHz, CD_2Cl_2, 300 K): $\delta = 121.0$ (q, $^1J_{C,F} = 291$ Hz), 78.4 ppm (m); ^{19}F NMR (376 MHz, CD_2Cl_2, 300 K): $\delta = -75.7$ (s, 54 F; CF_3), −184.8 ppm (s, 1 F; Al-F); ^{27}Al NMR (104 MHz, CD_2Cl_2, 300 K): $\delta = 37.5$ ppm (s br, $\omega_{1/2} = 3100$ Hz); ^{31}P NMR (101 MHz, CD_2Cl_2, 300 K): $\delta = -116.7$ (d, $^2J_{P,P} = 67.9$ Hz), 73.5 ppm (q, $^2J_{P,P} = 67.9$ Hz); IR (CsI plates, Nujol mull): $\tilde{\nu} = 288$ (m), 318 (mw), 331 (w), 347 (w), 376 (ms), 409 (m), 430 (ms), 543 (ms),491 (w), 536 (m), 569 (ms), 633 (s), 722 (s), 760 (mw), 810 (w), 863 (s), 953 (s), 974 (s) 1088 (mw, sh), 1152 (s), 1169 (s), 1217 (s), 1250 (s), 1303 cm^{-1} (s); Raman: $\tilde{\nu} = 193$, 222, 246, 289, 325, 346, 415, 432, 447, 468, 493, 539, 571, 753, 816, 987 cm^{-1}; ESI-MS: $[\{(CF_3)_3CO\}_3\text{-}Al\text{-}F\text{-}Al\{OC(CF_3)_3\}_3]^-$ (*m*/*z* 1483, 22 %) $[F\text{-}Al\{OC(CF_3)_3\}_3]^-$ (*m*/*z* 752, 100 %), $[Al\{OC(CF_3)_3\}_4]^-$ (*m*/*z* 968, 94 %), $[\{(CF_3)_3CO\}_3\text{-}Al\text{-}F\text{-}Al\{OC(CF_3)_2\}]^-$ (*m*/*z* 1247, 7 %), $[\{(CF_3)_3CO\}\text{-}Al\text{-}F_2\text{-}Al\text{-}\{OC(CF_3)_3\}_3)]^-$ (*m*/*z* 1501, 18 %).

Computational details: All computations were performed by using the program package TURBOMOLE 5.7.[46] All geometries were optimized at the (RI)-BP86/SV(P) level of theory.[47] The 28 core electrons of the Ag atom were replaced by a scalar relativistic pseudopotential.[48] For the computation of solvation enthalpies (solvent: CH_2Cl_2, with $\varepsilon = 8.93$ at 298 K and with $\varepsilon = 14.95$ at 195 K), the COSMO model was used.[49] To determine if a calculated structure was a local minimum at the PES, vibrational frequencies of all assessed species were computed.[50] These positions and intensities of the calculated frequencies were also used to simulate vibrational spectra by a superposition of Gauss-type functions. For the calculation of the NMR shielding tensors, a single-point calculation on the (RI)-BP86/SV(P) geometry were performed with the following basis sets: SVPalls2 for Ag atoms and SV(P) for P and S atoms. Entropic contributions to H(298 K/195 K) and G(298 K/195 K) were calculated with the module FreeH included with TURBOMOLE.

CCDC-625079–625082 contain the supplementary crystallographic data for compounds **2** (150 K), **7** (100 K and 283 K), **8** (130 K) of this paper. These data can be obtained free of charge from the Cambridge Crystallographic Data Centre via www.ccdc.cam.ac.uk/data_request/cif. Further information on the crystal structure investigations of α- and γ-P_4S_3 may be obtained from the Fachinformationszentrum Karlsruhe, 76344 Eggenstein-Leopoldshafen, Germany (fax: (+49)7247-808-666; e-mail: crysdata@fiz-karlsruhe.de, on quoting the depository numbers CSD-417154 and CSD-417155.

Acknowledgements

We thank Dr. Alain Razaname (Lausanne) for recording the ESI mass spectra. This work was supported by the DFG, the EPFL, the Albert-Ludwigs-Universität Freiburg and the Fonds der Chemischen Industrie.

[1] T. S. Cameron, A. Decken, I. Dionne, M. Fang, I. Krossing, J. Passmore, *Chem. Eur. J.* **2002**, *8*, 3386–3401.
[2] M. Di Vaira, M. Peruzzini, P. Stoppioni, *Inorg. Chem.* **1983**, *22*, 2196–2198.
[3] M. Gonsior, S. Antonijevic, I. Krossing, *Chem. Eur. J.* **2006**, *12*, 1997–2008.
[4] M. Scheer, L. J. Gregoriades, A. V. Virovets, W. Kunz, R. Neueder, I. Krossing, *Angew. Chem.* **2006**, *118*, 5818–5822; *Angew. Chem. Int. Ed.* **2006**, *45*, 5689–5693.
[5] I. Krossing, *J. Am. Chem. Soc.* **2001**, *123*, 4603–4604.
[6] I. Krossing, L. van Wüllen, *Chem. Eur. J.* **2002**, *8*, 700–711.
[7] A. W. Cordes, R. D. Joyner, R. D. Shores, E. D. Dill, *Inorg. Chem.* **1974**, *13*, 132–134.
[8] C. Aubauer, E. Irran, T. M. Klapötke, W. Schnick, A. Schulz, J. Senker, *Inorg. Chem.* **2001**, *40*, 4956–4965.
[9] M. Di Vaira, M. Peruzzini, P. Stoppioni, *J. Chem. Soc. Dalton Trans.* **1985**, 291–295; C. A. Ghilardi, S. Midollini, A. Orlandini, *Angew. Chem.* **1983**, *95*, 800–801; *Angew. Chem. Int. Ed.* **1983**, *22*, 1066–1074; E. Kuwabara, R. Bau, *Acta Crystallogr. Sect. C* **1994**, *50*, 1409–1411.
[10] M. Di Vaira, P. Stoppioni, *Coord. Chem. Rev.* **1992**, *120*, 259–279; L. Y. Goh, W. Chen, R. C. S. Wong, *Angew. Chem.* **1993**, *105*, 1838–1840; *Angew. Chem. Int. Ed.* **1993**, *32*, 1728–1729; O. J. Scherer, *Chem. Unserer Zeit* **2000**, *34*, 374–381; J. Wachter, *Angew. Chem.* **1998**, *110*, 782–800; *Angew. Chem. Int. Ed.* **1998**, *37*, 750–768.
[11] L. Y. Goh, W. Chen, R. C. S. Wong, K. Karaghiosoff, *Organometallics* **1995**, *14*, 3886–3896.
[12] G. Brunklaus, J. C. C. Chan, H. Eckert, S. Reiser, T. Nilges, A. Pfitzner, *Phys.Chem.Chem. Phys.* **2003**, *5*, 3768–3776.
[13] I. Krossing, A. Reisinger, *Coord. Chem. Rev.* **2006**, *250*, 2721–2744; *Chemistry with poly- and perfluorinated alkoxyaluminates: Gas-phase cations in the condensed phase? I. Krossing, A. Reisinger in Inorganic Chemistry in Focus II* (Eds.: G. Meyer, D. Naumann, L. Wesemann), Wiley-VCH, Weinheim, **2005**.
[14] K. Seppelt, *Z. Anorg. Allg. Chem.* **2003**, *629*, 2427–2430.
[15] A. Reisinger, W. Scherer, I. Krossing, unpublished results.
[16] A. Reisinger, F. Breher, D. V. Deubel, I. Krossing, unpublished results .
[17] I. Krossing, *Chem. Eur. J.* **2001**, *7*, 490–502.
[18] A. Adolf, M. Gonsior, I. Krossing, *J. Am. Chem. Soc.* **2002**, *124*, 7111–7116.
[19] I. de los Rios, F. Mani, M. Peruzzini, P. Stoppioni, *J. Organomet. Chem.* **2004**, *689*, 164–169; M. Di Vaira, I. de los Rios, F. Mani, M. Peruzzini, P. Stoppioni, *Eur. J. Inorg. Chem.* **2004**, 293–300.
[20] E. Guidoboni, I. de los Rios, A. Ienco, L. Marvelli, C. Mealli, A. Romerosa, R. Rossi, M. Peruzzini, *Inorg. Chem.* **2002**, *41*, 659–668.
[21] E. R. Andrew, A. Bradbury, R. G. Eades, *Nature* **1958**, *182*, 1659.
[22] W. P. Aue, J. Karhan, R. R. Ernst, *J. Chem. Phys.* **1976**, *64*, 4226–4227.
[23] A. Bax, R. Freeman, T. A. Frenkiel, *J. Am. Chem. Soc.* **1981**, *103*, 2102–2104.
[24] R. Benn, H. Grondey, C. Brevard, A. Pagelot, *J. Chem. Soc. Chem. Commun.* **1988**, 102–103; T. A. Early, B. K. John, L. F. Johnson, *J. Magn. Reson.* **1987**, *75*, 134–138; C. A. Fyfe, Y. Feng, H. Gies, H. Grondey, G. T. Kokotailo, *J. Am. Chem. Soc.* **1990**, *112*, 3264–3270; A. Lesage, C. Auger, S. Caldarelli, L. Emsley, *J. Am. Chem. Soc.* **1997**, *119*, 7867–7868.
[25] A. Lesage, M. Bardet, L. Emsley, *J. Am. Chem. Soc.* **1999**, *121*, 10987–10993.
[26] F. Fayon, D. Massiot, M. H. Levitt, J. J. Titman, D. H. Gregory, L. Duma, L. Emsley, S. P. Brown, *J. Chem. Phys.* **2005**, *122*, 194313.
[27] S. P. Brown, M. Perez-Torralba, D. Sanz, R. M. Claramunt, L. Emsley, *Chem. Commun.* **2002**, 1852–1853.
[28] T. Chattopadhyay, E. Gmelin, H. G. von Schnering, *J. Phys. Chem. Solids* **1982**, *43*, 925–932.
[29] T. K. Chattopadhyay, W. May, H. G. von Schnering, G. S. Pawley, *Z. Kristallogr.* **1983**, *165*, 47–64.
[30] H. L. Clever, E. F. Westrum, Jr., A. W. Cordes, *J. Phys. Chem.* **1965**, *69*, 1214–1219.
[31] M. Gardner, *J. Chem. Soc. Dalton Trans.* **1973**, 691–696.
[32] H. Gerding, J. W. Maarsen, P. C. Nobel, *Recueil des Travaux Chimiques des Pays-Bas et de la Belgique* **1957**, *76*, 757–786; J. O. Jensen, D. Zeroka, A. Banerjee, *Theochem* **2000**, *505*, 31–43.
[33] E. R. Andrew, W. S. Hinshaw, M. G. Hutchins, A. Jasinski, *Chem. Phys. Lett.* **1974**, *27*, 96–99.
[34] E. R. Andrew, W. S. Hinshaw, A. Jasinski, *Chem. Phys. Lett.* **1974**, *24*, 399–400.
[35] M. G. Gibby, A. Pines, W. K. Rhim, J. S. Waugh, *J. Chem. Phys.* **1972**, *56*, 991–995.
[36] R. K. Harris, P. J. Wilkes, P. T. Wood, J. D. Woollins, *J. Chem. Soc. Dalton Trans.* **1989**, 809–813.
[37] M. M. Maricq, J. S. Waugh, *J. Chem. Phys.* **1979**, *70*, 3300–3316; A. Schmidt, S. Vega, *J. Chem. Phys.* **1987**, *87*, 6895–6907.
[38] Y.-C. Leung, J. Waser, *Acta Crystallogr.* **1957**, *13*, 574–582; S. van Houten, A. Vos, G. A. Wiegers, *Recueil des Travaux Chimiques des Pays-Bas et de la Belgique* **1955**, *74*, 1167–1170.

[39] A. Bihlmeier, M. Gonsior, I. Raabe, N. Trapp, I. Krossing, *Chem. Eur. J.* **2004**, *10*, 5041–5051.
[40] T. S. Cameron, I. Dionne, H. D. B. Jenkins, S. Parsons, J. Passmore, H. K. Roobottom, *Inorg. Chem.* **2000**, *39*, 2042–2052; L. Glasser, H. D. B. Jenkins, *Chem. Soc. Rev.* **2005**, *34*, 866–874.
[41] S. Brownridge, I. Krossing, J. Passmore, H. D. B. Jenkins, H. K. Roobottom, *Coord. Chem. Rev.* **2000**, *197*, 397–481; L. J. Gregoriades, H. Krauss, J. Wachter, A. V. Virovets, M. Sierka, M. Scheer, *Angew. Chem.* **2006**, *118*, 4295–4298; *Angew. Chem. Int. Ed.* **2006**, *45*, 4189–4192.
[42] I. Krossing, H. Brands, R. Feuerhake, S. Koenig, *J. Fluorine Chem.* **2001**, *112*, 83–90.
[43] I. Krossing, A. Bihlmeier, I. Raabe, N. Trapp, *Angew. Chem.* **2003**, *115*, 1569–1572; *Angew. Chem. Int. Ed.* **2003**, *42*, 1531–1534.
[44] I. Krossing, I. Raabe, N. Trapp, S. Müller, M. Kaupp, unpublished results .
[45] A. L. Van Geet, *Anal. Chem.* **1970**, *42*, 679–680.
[46] R. Ahlrichs, M. Bär, M. Häser, H. Horn, C. Kölmel, *Chem. Phys. Lett.* **1989**, *162*, 165–169.
[47] A. D. Becke, *J. Chem. Phys.* **1993**, *98*, 5648–5652; J. P. Perdew, *Phys. Rev. B* **1986**, *33*, 8822–8824.
[48] D. Andrae, U. Häussermann, M. Dolg, H. Stoll, H. Preuss, *Theor. Chim. Acta* **1990**, *77*, 123–141.
[49] A. Klamt, G. Schüürmann, *J. Chem. Soc. Perkin Trans. 1* **1993**, 799–805.
[50] P. Deglmann, F. Furche, *J. Chem. Phys.* **2002**, *117*, 9535–9538; P. Deglmann, F. Furche, R. Ahlrichs, *Chem. Phys. Lett.* **2002**, *362*, 511–518; P. Deglmann, K. May, F. Furche, R. Ahlrichs, *Chem. Phys. Lett.* **2004**, *384*, 103–107.

Received: December 28, 2006
Revised: March 29, 2007
Published online: July 6, 2007

